SSRG International Journal of Applied Chemistry
ISSN: 2393 – 9133 / https://doi.org/10.14445/23939133/IJAC-V13I2P103

Volume 13 Issue 2, 17-33, May-Aug 2026

Original Article

From Ligand to Bioactive Complex: Crystal Structure of ligand and DPPH Radical-Scavenging Enhancement in an Iron(III) Hydrazone Schiff Base

Abdoul Sall[1], Ousmane Sall[2], Moussa Faye[1], Alassane Saïdou Diallo[1], Farba Bouyagui Tamboura[1], Ibrahima Elhadj Thiam[2], Moussa Dieng[1]*, Mohamed Gaye[2]

[1]*Department of Chemistry, Cheikh Anta Diop University, Dakar, Senegal.*
[2]*Department of Chemistry, Alioune Diop University, Bambey, Senegal.*

[*]*Corresponding Author : moussa.dieng@uadb.edu.sn*

Received: 06 June 2026 Revised: 15 July 2026 Accepted: 08 August 2026 Published: 30 August 2026

Abstract *- A new HYDRAZONE SCHIFF BASE, N'-[(1E)-1-(5-bromo-2-hydroxyphenyl)Ethylidene]Pyridine-3-Carbohydrazide (H_2L), was synthesized from 5-bromo-2-Hydroxyacetophenone and Nicotinic acid Hydrazide, and its Iron(III) complex was prepared. The ligand was characterized by single-crystal X-ray diffraction, $^1H/^{13}C$ NMR, and both compounds were studied by IR, UV-Vis, and molar conductivity measurements. Spectroscopic data indicate that, following amide-iminol tautomerization, the ligand coordinates through the iminol oxygen, azomethine nitrogen, and pyridine nitrogen atoms, giving an octahedral iron(III) center that is non-electrolytic and stable in DMF. DPPH assays showed enhanced radical-scavenging activity for the complex relative to the free ligand (IC_{50} = 2.6 vs 4.8 mg mL^{-1}), though both remained less active than ascorbic acid. The compounds also displayed selective antibacterial activity, favoring Gram-positive strains (S. aureus, E. faecalis) over E. coli. These results highlight the role of metal coordination in enhancing the bioactivity of hydrazone Schiff bases and support iron(III) complexes as promising candidates for new bioactive coordination compounds.*

Keywords *- Schiff Base, Iron(Iii) Complex, Single-Crystal X-Ray Diffraction, Coordination Chemistry, Antibacterial Activity, Antioxidant Activity.*

1. Introduction

Cobalt and copper complexes derived from symmetrical Schiff base ligands have attracted considerable attention over the past decades because of their remarkable biological properties [1-2]. Iron and manganese complexes also occupy a prominent position in coordination chemistry owing to their structural diversity and versatile redox behavior. Their coordination with azomethine ligands, such as hydrazones and thiosemicarbazones, leads to the formation of stable coordination systems exhibiting promising catalytic and biological properties [3-4].

Studies on the antimicrobial activities of novel cobalt [5] and copper [6] Schiff base complexes have contributed significantly to the search for new antimicrobial agents. Indeed, many of these compounds exhibit pronounced antibacterial [7], antifungal, and antitumor activities [8], making them highly attractive for medical and pharmaceutical applications [9]. Furthermore, numerous investigations have demonstrated that the coordination of Schiff base ligands to metal ions often enhances their biological activities compared with those of the corresponding free ligands [10].

The present study reports the synthesis of a Schiff base ligand and its metal complex, together with their spectroscopic and structural characterization, as well as an evaluation of their antibacterial and antioxidant activities.

2. Experimental

2.1. Synthesis of N'-[(1E)-1-(5-Bromo-2-hydroxyphenyl)ethylidene]pyridine-3-carbohydrazide

2.1.1. Reaction Scheme

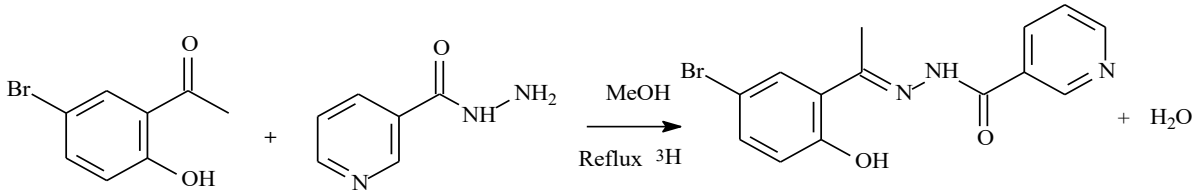

Scheme 1 : Formation of N'-[(1E)-1-(5-Bromo-2-hydroxyphenyl)ethylidene]pyridine-3-carbohydrazide

2.1.2. Procedure

A solution of 5-bromo-2-hydroxyacetophenone (6 mmol) was prepared in 20 mL of ethanol in a round-bottom flask. After complete dissolution, a solution containing 6 mmol of nicotinohydrazide, previously dissolved in methanol, was added, followed by a few drops of glacial acetic acid as a catalyst. The reaction mixture was refluxed for 3 hours under continuous stirring. Upon cooling to room temperature, a yellow precipitate formed and was collected by filtration, washed twice with 10 mL portions of cold ethanol, and dried in air to afford the desired Schiff base ligand.

Yield : 85 %, Melting temperature : 260°C
Anal. Calc. (%) for $C_{14}H_{12}BrN_3O_2$: C: 50.32, H: 3.62, N: 12.56, Br: 23.91.

Found: C : 50.55, H : 3.16, N : 12.12, Br : 23.85.

NMR ^{1}H : (δ, ppm) : 3.835 (s, 3H, CH_3) ; 5.752-7.63 (m, 7H, Ar-H et Py-H) ; 10.80 (s, 1H, Ar-OH) ; 11.867 (s, 1H, NH).
NMR ^{13}C : (δ, ppm): 14.806 (CH_3); 110.097-157.568 (C_{Ar}, C_{Py}); 158.350 (C=N); 163.603 (C=O).

2.2. Synthesis of the Iron(III) Complex

2.2.1. General Synthetic Procedure

Iron(III) perchlorate hexahydrate (1 mmol) was dissolved in 10 mL of ethanol in a beaker. To this solution, 1 mmol of the Schiff base ligand H_2L was added under continuous magnetic stirring. The reaction mixture was stirred at room temperature for 30 minutes and then filtered. The resulting filtrate was left to evaporate slowly in air. The solid complex obtained was collected, washed twice with 10 mL portions of diethyl ether, and dried in a desiccator over P_2O_5. The physical characteristics of the synthesized complex are summarized in table 1.

Table 1. Melting point, appearance, color and yield of the complex.

Metal Salt	Compound	Yield (%)	MP (°C)	Color, Appearance
$Fe(ClO_4)_3.6H_2O$	$\{Fe(HL)(ClO_4)_2\}$	61	>260	Black precipitate

3. Results and Discussion

The topological structure of the ligand is shown in the following scheme.

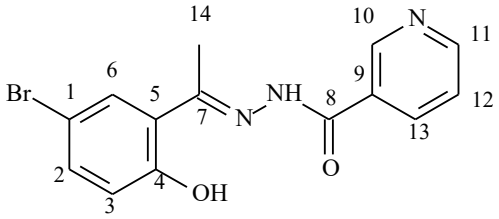

Scheme 2. Structure of the H_2L ligand.

3.1. Infrared Spectroscopic Study of the H_2L Ligand

The IR spectrum of H_2L shows intense bands in the 1417-1557 cm^{-1} region, assigned to the C=N and C=C stretching vibrations of the pyridine rings [11], and a strong band at 1597 cm^{-1} attributed to the azomethine ν(C=N) stretch [12], confirming Schiff base formation. The disappearance of the ν(C=O) band of the starting 5-bromo-2-hydroxyacetophenone (~1660 cm^{-1}), together with the appearance of a new amide carbonyl band at 1661 cm^{-1} from the hydrazide moiety, further confirms formation of the ligand.

Bands at 1289 and 1102 cm^{-1} are assigned to the phenolic ν(C–O) and ν(N–N) vibrations, respectively [13], while a medium-intensity band at 3211 cm^{-1} corresponds to ν(O–H) of the phenolic group [14]. The spectrum also displays the aromatic ν(C–H) vibration of the pyridine rings at 3056 cm^{-1} and the pyridine ring deformation mode at 622 cm^{-1}.

3.2. Infrared Spectroscopic Study of the Complex

In free H_2L, the ν(C=O) and ν(C=N) bands appear at 1642 and 1597 cm^{-1}, respectively. Upon complexation, the ν(C=O) band disappears entirely, while a new band assigned to the conjugated ν(>C=N–N=C<) system appears near 1590 cm^{-1}, indicating amide-iminol tautomerization followed by deprotonation and coordination through the resulting iminol oxygen [15-17]. This mode is further supported by the characteristic ν(NCO$^-$) vibrations at 1514-1527 and 1254-1321 cm^{-1} [18-20]. Coordination through the azomethine nitrogen is evidenced by the downshift of ν(C=N), and through the ν(N–N) shift to 1075-1090 cm^{-1}, while shifts in the pyridine ring vibrations confirm participation of the pyridine nitrogen [21-23]. Broad bands in the 3000-3400 cm^{-1} region are assigned to coordinated and/or lattice water, and new low-frequency bands at 456-577 cm^{-1} are attributed to ν(M–O) and ν(M–N), confirming the involvement of oxygen and nitrogen donor atoms in the coordination sphere [24].

Table 2. Infrared spectral data for the complex and H_2L ligand

Compounds	ν(C=O)	ν(C=N)	$\nu(C\text{-}O)_{ph}$	$\nu(C=N)_{py}$	δ(C=N)	ν(N–N)	ν(NCO$^-$)	ν(C=N–N=C)
H_2L	1642	1597	1289	1417-1557	675	1102	-	-
$\{Fe(HL)(ClO_4)_2\}$	-	1590	1286	1414-1527	645	1075	1514-1527	1495-1321

3.3. NMR Spectroscopy

3.3.1. ^{1}H NMR

The ^{1}H NMR spectrum of the H_2L ligand, recorded in DMSO-d_6, is fully consistent with the proposed molecular structure and displays the characteristic proton resonances expected for the Schiff base.

A singlet observed at δ 2.52 ppm is assigned to the methyl protons (–CH_3, C14). This signal overlaps with the residual resonance of DMSO-d_6, which appears at δ 2.50 ppm. A sharp signal at δ 3.34 ppm is attributed to residual water in the solvent [25-26].

In the aromatic region, between δ 6.89 and 9.09 ppm, a series of multiplets integrating for a total of seven protons is observed, corresponding to the three protons of the trisubstituted benzene ring and the four protons of the pyridine ring, in agreement with the proposed structure.

A broad singlet at δ 11.61 ppm is assigned to the amide N–H proton (–NH–CO–). The phenolic hydroxyl proton appears as a sharp, highly deshielded singlet at δ 13.37 ppm, integrating for one proton. Its pronounced downfield chemical shift is attributed to the formation of a strong intramolecular O–H···N hydrogen bond between the phenolic hydroxyl group and the neighboring imine nitrogen atom, a characteristic feature of salicylidene-derived hydrazone ligands.

3.3.2. ^{13}C NMR

The ^{13}C NMR spectrum of the H_2L ligand, recorded in DMSO-d_6, exhibits thirteen distinct resonances for the fourteen carbon atoms of the molecule, indicating that two aromatic carbon atoms possess nearly identical chemical shifts.

The resonance at δ 14.80 ppm is assigned to the methyl carbon (C14). The most downfield signal, observed at δ 163.60 ppm, is attributed to the azomethine carbon (C9, C=N), confirming the formation of the Schiff base.

The phenolic carbon bonded to the hydroxyl group (C–OH) and the amide carbonyl carbon (C=O) resonate at δ 158.35 and 157.56 ppm, respectively. The remaining signals, appearing in the δ 110.09-152.97 ppm range, are assigned to the sp^2-hybridized carbon atoms of the aromatic benzene and pyridine rings.

A characteristic intense septet centered at approximately δ 39.5-40.0 ppm arises from the DMSO-d_6 solvent and is therefore not associated with the ligand.

Table 3. Signal assignments for the ^{1}H and ^{13}C NMR spectra of ligand H_2L.

Attribution	δ ^{1}H (ppm), Multiplicity, Integration	δ ^{13}C (ppm)
OH (phenolic)	13.37 ppm (s, 1H)	-
(–NH–CO–) (amide)	11.62 ppm (s, 1H)	-
C=O (amide)	-	157.56
C=N (imine)	-	163.60
CH_3 (methyl)	2.50 ppm (s, 3H)	14.80
C-OH (aromatic)	-	158.35
aromatic/pyridinic protons & carbons	6.89-9.09 ppm (m, 7H)	110.10-152.97

Table 4. Conductometric data for the complex derived from ligand H_2L

Complex	Fresh solution ($\Omega^{-1}.cm^2.mol^{-1}$)	15 days later ($\Omega^{-1}.cm^2.mol^{-1}$)	Electrolytes
{Fe(HL)(ClO_4)$_2$}	22.29	22.04	Neutral

4. Conductometric Study

The following table 4 presents data obtained from molar conductivity measurements of the fresh solution and the solution after fifteen (15) days of storage.

The molar conductivities of 1.0 x 10^{-3} mol L^{-1} solutions of all the synthesized complexes were measured in N, N-Dimethylformamide (DMF). Two series of measurements, performed at an interval of 15 days, were carried out to determine the electrolytic nature of the complexes and to evaluate their stability in solution.

The freshly prepared solutions exhibited molar conductivity values in the range of 20-35 $\Omega^{-1}.cm^2.mol^{-1}$, which are consistent with those expected for non-electrolytic (neutral) complexes in DMF. Moreover, no significant change in the molar conductivity values was observed after two weeks, indicating that the complexes remain stable in solution over this period [27].

5. UV-Visible Spectroscopic and Magnetic Data for the Ligand and the Complex

The UV-Visible spectrum of the iron(III) complex exhibits an intense absorption band at 352 nm, which is assigned to the π → π* electronic transition associated with the aromatic system of the Schiff base ligand. A second absorption band centered at 452 nm is attributed to the n → π* transition involving the azomethine and carbonyl chromophores of the coordinated ligand [28,29]. In addition, the spectrum of {Fe(HL)(ClO_4)$_2$} displays a broad absorption band at approximately 520 nm, which is assigned to a d-d transition of the Fe(III) ion in an octahedral coordination environment [30]. The presence of this band is consistent with the proposed octahedral geometry around the iron(III) center.

Table 5. UV-visible and magnetic data for the complex

Compound	λ (nm)	Attribution	μ_{eff} (μ_B)
{Fe(HL)(ClO_4)$_2$}	352	π → π*	5.8
	452	n → π*	
	520	d → d	

6. Crystal Structure Determination of H_2L

The crystallographic data and refinement details for ligand H_2L are listed in Table 6.

Table 6. Crystallographic data and structure refinement for ligand H_2L.

Parameter	Value
Identification code	H_2L
Formula	$C_{14}H_{13}BrN_3O_2$
Formula weight	335.18
Temperature /K	100
Crystal system	Monoclinic
Size (mm)	0.22 x 0.1 x 0.09
Space group	$P2_1/c$
a/Å	4.8700(1)
b/Å	16.3539(3)
c/Å	16.5160(4)
α/°	90
β/°	93.948(2)
γ/°	90
Cell volume (Å^3)	1312.27
Z	4
μ/mm^{-1}	3.15
Density (Mgm^{-1})	1.691
θ(°)	2.5-37.6
R_{int}	0.035
F(000)	617.605
Radiation	Mo *K*α radiation, λ = 0.71075 Å
h, k, l ranges	-8→8, -27→27, -27→27
Reflections collected	32602
Independent reflections	6351
Data/restraints/parameters	188
Final *R* Indices [$I > 2\sigma(I)$]	0.029
Final *R* Indices [all the data]	0.067
Δρmax, Δρmin (e Å^{-3})	0.78, -0.56
Gof	1.00

Table 7. Hydrogen-bond geometry (Å,°)

D—H···A	D—H	H···A	D···A	D—H···A
N2—H2a···O2^{i}	0.84(2)	2.05(2)	2.8749(12)	167(2)
O1—H1···N1	0.80(2)	1.80(2)	2.5280(13)	150(2)

Symmetry code : (i) x-1, y, z.

Crystals suitable for X-ray diffraction were grown by slow evaporation of a methanolic solution of the ligand. Details of the crystal structure solution, refinement and hydrogen-bond geometry are given respectively in tables 6 and 7. A suitable single crystal was selected and mounted on a Bruker APEX-II CCD diffractometer using graphite-monochromated Mo Kα radiation (λ = 0.71073 Å). All data were corrected for Lorentz and polarization effects; no absorption correction was applied. Hydrogen atoms on water molecules and NH groups were located from difference Fourier maps and refined isotropically [31]. Remaining hydrogen atoms were geometrically optimized and refined using a riding model with AFIX instructions.

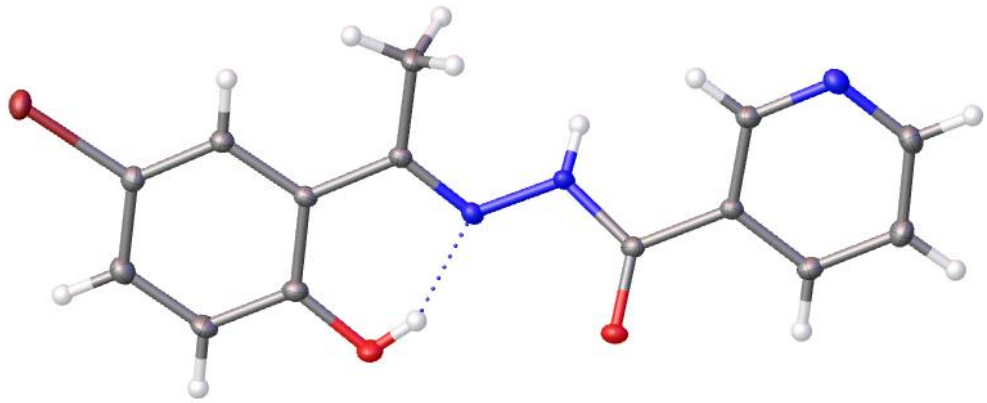

Fig. 1 Crystal Structure of H_2L Ligand

7. Antibacterial Activities Study

The antibacterial activity of the ligand (E)-1-(pyridin-2-yl)-2-(pyridin-2-ylmethylene)hydrazone (**HL**) and its lanthanide complexes with Nd(III), Sm(III), Tb(III), Er(III), Ce(III) and Pr(III) was extensively investigated by M. Ndiaye-Gueye *et al.* [32]. The antibacterial properties of these compounds were evaluated using the agar diffusion method described by Treki [33]. Three standard bacterial strains obtained from the Bacteriology Laboratory of the Aristide Le Dantec University Hospital (Dakar, Senegal) were used: *Escherichia coli*, *Pseudomonas aeruginosa*, and *Staphylococcus aureus*.

7.1. Determination of the Minimum Inhibitory Concentrations (MICs)

The different bacterial strains were subcultured by the streak plate method and incubated at 37°C for 24 hours to obtain fresh cultures with well-isolated colonies. The colonies were subsequently suspended in sterile distilled water to prepare the bacterial inoculum. The turbidity of each suspension was adjusted to the 0.5 McFarland standard, corresponding to the recommended initial bacterial cell density.

The preliminary screening results were subsequently used to determine the Minimum Inhibitory Concentrations (MICs) of the active compounds. The concentrations 3, 3/2, 3/4, 3/8, etc., correspond to a two-fold serial dilution of the initial stock solution of each dry extract dissolved in DMSO at a concentration of 6 mg mL^{-1}.

The MIC assay was performed using the agar well diffusion method. Mueller-Hinton agar plates were inoculated by flooding with the standardized bacterial suspension. A template consisting of 10 rows of 12 wells, each approximately 6 mm in diameter, was used to evaluate the antibacterial activity against the three reference bacterial strains.

Each well received 100 µL of the bacterial inoculum followed by 100 µL of the test solution at the following concentrations: 3 mg/mL; 3/2 (1.5 mg/mL); 3/4 (0.75 mg/mL); 3/8 (0.375 mg/mL); 3/16 (0.187 mg/mL); 3/32 (0.094 mg/mL); 3/64 (0.047 mg/mL); 0.023 mg/mL; 0.012 mg/mL; 3/992 (0.006 mg/mL).

Columns 1 and 2 served as the positive and negative controls, respectively. The positive control wells received 10 µL of ciprofloxacin solution, whereas the negative control contained only the solvent DMSO. After inoculation, the Petri dishes were gently rotated by approximately 60° to ensure homogeneous distribution of the bacterial suspension.

Following a 30 minutes diffusion period at room temperature, the plates were incubated at 37°C for 24 hours. The presence or absence of bacterial growth inhibition was evaluated on the following day by visual inspection of the inhibition zones [34]. The antibacterial activity was interpreted according to the criteria proposed by Duraffourd *et al.***,** Ponce *et al.* [35, 36].

The Minimum Inhibitory Concentration (MIC) was defined as the lowest concentration of the tested compound capable of inhibiting visible bacterial growth. The MIC values obtained for each ligand and lanthanide complex were subsequently used to compare their relative antibacterial effectiveness against the tested bacterial strains.

7.2. Results and Discussion

The antibacterial activities of the europium, ytterbium, lanthanum, praseodymium, samarium, erbium, terbium, neodymium, and cerium complexes were evaluated against three reference bacterial strains: *Escherichia coli*, *Pseudomonas aeruginosa*, and *Staphylococcus aureus*. The obtained results (table 8) demonstrate that all compounds exhibited antibacterial activity against the tested microorganisms.

Against *Pseudomonas aeruginosa*, the free ligand (HL) together with the europium, ytterbium, and lanthanum complexes exhibited the highest antibacterial activity, with MIC values of 0.094 mg mL^{-1}**.** The praseodymium and samarium complexes displayed comparable antibacterial activity, with MIC values of 0.094 mg mL^{-1}, whereas the erbium, terbium, neodymium, and cerium complexes were

less active, exhibiting MIC values ranging from 0.187 to 0.375 mg mL^{-1}.

For *Escherichia coli*, the lanthanum and praseodymium complexes showed the strongest antibacterial effect, with identical MIC values of 0.047 mg mL^{-1}. The ligand HL, together with the europium, samarium, erbium, and cerium complexes, exhibited intermediate activity (MIC = 0.094 mg mL^{-1}), whereas the ytterbium, terbium, and neodymium complexes were less active, each displaying an MIC of 0.187 mg mL^{-1}.

In contrast, all investigated compounds exhibited similar antibacterial activity against *Staphylococcus aureus*. The ligand HL and the europium, ytterbium, lanthanum, praseodymium, and samarium complexes showed identical MIC values of 0.75 mg mL^{-1}, whereas the erbium, terbium, neodymium, and cerium complexes exhibited MIC values greater than 0.75 mg mL^{-1}, indicating comparatively lower antibacterial activity toward this Gram-positive strain.

The MIC values obtained for all investigated compounds are summarized in table 8.

Table 8. Minimum inhibitory concentrations (MICs) of HL and its lanthanide complexes against the tested bacterial strains (mg mL^{-1})

Reference	HL	Eu	Yb	La	Pr	Sm	Er	Tb	Nd	Ce
E. coli	0.094	0.094	0.187	0.047	0.047	0.094	0.094	0.187	0.187	0.094
Pseudo	0.094	0.094	0.094	0.094	0.094	0.094	0.187	0.375	0.375	0.375
S. aureus	0.75	0.75	0.75	0.75	0.75	0.75	> 0.75	> 0.75	> 0.75	> 0. 75

Overall, the investigated compounds exhibited measurable antibacterial activity against all three reference bacterial strains. The highest susceptibility was observed for *Escherichia coli*, for which the lanthanum and praseodymium complexes displayed the lowest MIC values (0.047 mg mL^{-1}), indicating superior antibacterial potency compared with the remaining compounds. The ligand HL and the other lanthanide complexes also demonstrated appreciable activity, with relatively similar MIC values.

These findings indicate that coordination of the hydrazone ligand to lanthanide(III) ions preserves, and in some cases enhances, its antibacterial properties. The observed differences among the complexes are likely related to variations in the ionic radius, coordination environment, and electronic characteristics of the individual lanthanide ions, which may influence the interaction of the complexes with bacterial cells.

The antimicrobial evaluation, therefore, demonstrates that both the free ligand and its lanthanide complexes possess promising antibacterial activity against representative Gram-negative (*Escherichia coli* and *Pseudomonas aeruginosa*) and Gram-positive (*Staphylococcus aureus*) bacteria. These results highlight the potential of these coordination compounds as candidates for further investigations into the development of novel antimicrobial agents.

7.3. Sensitivity Test Protocol about H_2L

The diffusion method is one of the oldest approaches to determining the sensitivity of bacteria to antibiotics or natural or synthetic compounds and remains one of the most routinely used methods. It is suitable for the majority of pathogenic bacteria, including slow-growing bacteria; it allows a variety in the choice of antibiotics and does not require any special equipment. Like most agar diffusion techniques, the EUCAST method is standardized, based on the principles defined in the report of the International Collaborative Study of Antimicrobial Susceptibility Testing (1972), but also on the experience of experts around the world.

7.3.1. Biology Antimicrobial Test

The antimicrobial activity of the synthesized compounds was studied *in vitro* using four reference bacterial strains, such as two Gram (+): *E. faec*alis ATCC 29212 and *S. aureus* ATCC 38213; two Gram (–): *E. coli* NCTC 25923 and *P. aeruginosa* ATCC 27853; and one yeast, *C. albicans* ATCC 24433. Erythromycin and tetracycline were used as reference compounds.

7.3.2. Inoculum Preparation

The microorganisms were first inoculated into the peptone medium and incubated at 37°C for 24 hours. After 24 hours of incubation, all microbial strains had grown in their respective media. From the cultures obtained, a microbial suspension in salt solution was made until the inoculum was estimated at 1.5 x108 CFU/mL based on a turbidity of 0.5 McFarland. The turbidity was measured using a densitometer.

7.4. MTT Assay Protocol

After trypsinization and counting, cells were seeded at 10 000 cells per well in a 96-well plate. 24 hours later, the compounds were added at different concentrations ranging from 0.0005 to 10 µg/mL in sextuplicate and incubated for 72 hours at 37°C. DMSO was used as a negative control, and carboplatin as a positive control. MTT (0.5 mg/mL) was then added, and the plate was incubated for an additional hour. After washing, intracellular formazan crystals were dissolved in 100 µL of DMSO and absorbance was measured at 570 nm using a Multiskan® FC plate reader (Thermo Scientific). Cell viability was then estimated in percentage of control cells treated with DMSO alone. Results are expressed as mean ± standard deviation (SD). Chi-square Test were performed using GraphPad Prism to determine differences. P value < 0.05 was considered statistically significant. IC_{50} was determined using the Quest Graph™ IC_{50} Calculator software [37].

7.5. Media Preparation

7.5.1. Preparation of MH Medium

19 g of Muller Hinton Agar were weighed using a precision balance, then suspended in 500 mL of distilled water and homogenized using a magnetic bar. The medium is then sterilized in an autoclave at 121°C for 15 minutes, then cooled in a marri bath to 45°C. Then the medium was poured into the sterile square petri dishes to a uniform thickness of approximately 4 mm, and the agar was allowed to settle at room temperature before putting them in the incubator at 37°C for 24 hours before use.

7.5.2. Preparation of Colombia Agar

This medium was used to perform microbial culture. 20 g of Columbia powder were suspended in 500 mL of distilled water and then homogenized using a magnetic stirrer. The mixture is then placed in the autoclave at 121°C for 15 minutes, then cooled in a water bath at 45°C. The medium was poured into round petri dishes under a hood and allowed to solidify at room temperature. These were stored in an oven at 37°C for 24 hours to test their sterility before use. The boxes must not be dried out. If they must be used after 7 days, they must be stored at 4-8°C in a sealed plastic bag.

7.6. Microbial Culture and Purification

The dial method was used to carry out strain purification. 20 µL of the microbial suspension was placed on the Colombia agar medium, using a seeding loop, and the drop was scraped to the middle of the dish carefully to avoid scratching the agar. Using the ring of the handle, trace tight streaks on the first dial (in the most delicate way so as not to damage the agar). Then we turn the box towards the second dial, and we trace it in the same way as the first. We turn the box towards the third dial, we seed it this time with loose but distant streaks which do not overlap the previous deposit. The plates were then incubated at 37°C at 5% CO_2 for 24 hours.

7.7. Preparation of the Inoculum

From a visible microbial culture carried out on Colombian agar medium, produce a bacterial suspension in saline solution (PBS) to achieve a turbidity equivalent to that of the 0.5 standard from the McFarland range. To do this, take several colonies of the same morphology (if possible) to avoid selecting an atypical variant using a seed loop, and suspend these colonies in 10 mL of PBS.

The bacterial suspension is standardized using the 0.5 McFarland control. A heavy inoculum results in smaller diameters and vice versa. It is recommended to use a spectrophotometer to adjust the inoculum. This device must be calibrated against a standard from the McFarland range according to the manufacturer's recommendations. The turbidity of the bacterial suspension can also be compared with the naked eye to that of the 0.5 standard from the McFarland range. In this case, shake the turbidity standard vigorously on a VortexR before use (some commercial standards are gelled and should not be shaken; follow the manufacturer's recommendations).

7.8. Inoculation of the Agar and Deposition of the Impregnated Discs

The bacterial inoculum should ideally be used within 15 minutes of its preparation. Ten milliliters of inoculum are poured onto the surface of the poured and solidified culture medium (Muller-Hinton). The surface is covered completely; the excess is removed and thrown into the bleach. The plates were incubated for 1 hour before placing the disks.

The standard antibiotic disks of Doripenem, erythromycin (10 µg/disc) and Ceftriaxone (30 µg/disc) with diameters of 6 mm were used as positive controls and DMSO to prepare the dilutions of the different extracts was used as a negative control.

The tests were carried out on impregnated discs with a diameter of 6 mm, and the discs were impregnated with 40 µL of the solution to be evaluated with a concentration of 10 mg/mL).

The discs were firmly placed on the surface of the inoculated and dried agar. Contact with the surface should be close. The discs, once deposited, cannot be moved because the diffusion of antibiotics is very rapid. The number of discs placed per box is limited due to the overlapping of the inhibition zones and to limit interference between the compounds.

The boxes were turned over and incubated for 24 hours at 37°C at 5% CO_2. The antibacterial activity was evaluated by measuring the inhibition zone.

Fig. 2 The antibacterial activity

Table 9. Strains tested and Drugs tested

Strains Tested	Drugs Tested
Enterococcus faecalis ATCC 29212 (G+) (E. Faecalis)	H_2L
Pseudomonas aeruginosa ATCC 27853 (G-) (P. aerus)	$\{Fe(HL)(ClO_4)_2\}$

Table 10. Inhibition diameters (mm)

Strains / Drugs (C: mg /mL)	Staph aureus ATCC 38213 (G+)	E. coli NCTC 25923 (G-)	E. Faecalis ATCC 29212 (G+)	P. aerus ATCC 27853 (G-)
H_2L 10 mg/mL	10	10	7	NA
$\{Fe(HL)(ClO_4)_2\}$10 mg/mL	15	10	16	NA
DMSO	NA	NA	NA	NA
Doripenem : 10 µg	28	23	32	25
Ceftriaxone : 30 µg	NA	14	7	NA

NA: No Activity

Table 11. Minimum inhibitory concentration MIC

Strains / Drugs (C: mg /mL)	Staph aureus ATCC 38213 (G+)	E. coli NCTC 25923 (G-)	E. Faecalis ATCC 29212 (G+)	P. aerus ATCC 27853 (G-)
H_2L	5	10	ND	ND
$\{Fe(HL)(ClO_4)_2\}$	ND	ND	ND	ND
DMSO	NA	NA	NA	NA
Doripenem : 10 µg	28	23	32	25
Ceftriaxone : 30 µg	NA	14	7	NA

ND: Not Determined, NA: No Activity

The strains used for susceptibility testing are as follows

- Staphylococcus aureus ATCC 38213 (Gram positive)
- Escherichia coli NCTC 25923 (Gram negative)
- Enterococcus faecalis ATCC 29212 (Gram positive)
- Pseudomonas aeruginosa ATCC 27853 (Gram negative)

7.9. Bibliographic Study of Strains used in Sensitivity Tests

7.9.1. Staphylococcus Aureus ATCC 38213

Staphylococcus aureus is a Gram-positive cocci bacteria, a widely distributed opportunistic pathogen.

- Clinical interest: responsible for skin, pulmonary, osteo articular and septicemic infections
- Use in microbiology: strain ATCC 38213 is a reference strain frequently used for the evaluation of antibiotic sensitivity in agar diffusion tests and MICs. It serves in particular as quality control in the standardized CLSI and EUCAST protocols.
- Particularity: this strain is sensitive to many antibiotics, which makes it a good comparative model for testing new antimicrobial molecules.

7.9.2. Escherichia coli NCTC 25923

E. coli is a Gram-negative bacillus of the Entero bacteriaceae family, widely present in the human and animal intestinal microbiota.

- Clinical interest: certain commensal strains are harmless, but pathogenic strains are responsible for urinary, gastrointestinal, septicemic and meningeal infections.
- Use in microbiology: the NCTC 25923 strain is a reference strain used for quality control of sensitivity tests, in particular for antibiotics targeting Gram-negative bacteria.
- Special feature: this standardized strain makes it possible to compare the diffusion and effectiveness of antimicrobial compounds with international reproducibility.

7.9.3. Enterococcus faecalis ATCC 29212

Enterococcus faecalis is a Gram-positive cocci, often present in human intestinal flora.

- Clinical interest: it is involved in urinary infections, endocarditis and nosocomial infections.
- Use in microbiology: the ATCC 29212 strain is used as a standard control for determining the MIC of antibiotics. It is recommended by the CLSI for the validation of diffusion and dilution tests.
- Particularity: its relative tolerance to classic antibiotics makes it a reference strain for evaluating new molecules against resistant Gram-positive bacteria.

7.9.4. Pseudomonas Aeruginosa ATCC 27853

Pseudomonas aeruginosa is a non-fermentative Gram-negative bacillus, ubiquitous in humid environments.

- Clinical interest: major opportunistic pathogen, particularly feared in nosocomial infections (burns, pneumonia, septicemia). It has high natural resistance to many antibiotics.

- Use in microbiology: the ATCC 27853 strain is a reference strain used to evaluate the effectiveness of antimicrobial agents against non-fermentative Gram-negative bacilli. It is also a quality control for diffusion tests (CLSI, EUCAST).
- Special feature: it is a standardized sensitive strain, which allows the performance of antibiotics active on Pseudomonas to be compared.

This bibliography shows that the four strains chosen represent a relevant panel:

- Gram négatif (Escherichia, Pseudomonas)
- Quality control strains standardized by ATCC and NCTC, internationally recognized

7.9.5. Results and Discussions

Staphylococcus aureus ATCC 38213

- Role: Gram-positive reference strain often used as quality control in antibiotic sensitivity tests, notably by the disk diffusion method (Kirby-Bauer) or MICs (CLSI, EUCAST).
- Quality: described as a low producer of β-lactamases, sensitive to standard antibiotics
- Normative use: frequently referenced in CLSI and EUCAST standards as a QC strain for validation of media (Mueller-Hinton) and diffusion tests

Escherichia coli NCTC 25923

- Role: Gram-negative strain, used as a control strain (wild-type) to validate sensitivity tests (disk diffusion in particular).
- Quality: sensitive too many common antibiotics (neomycin, colistin, kanamycin, gentamicin, chloramphenicol, cephalosporins, etc.)

Enterococcus faecalis ATCC 29212

- Role: Gram-positive control strain, sensitive to vancomycin, widely used as QC for antibiogram tests (diffusion, dilution, etc.)
- Characterization: sequenced genome (~3 Mb, G+C ≈ 37%), isolate initially collected from a human urine sample
- QC value: validated in multicenter studies for diffusion and microdilution tests. Established control zones (gentamicin 16-22 mm, streptomycin 14-19 mm)

Pseudomonas Aeruginosa ATCC 27853

- Role: non-fermentative Gram-negative strain, reference for evaluating the effectiveness of antibiotics against this genus, particularly in diffusion tests.
- Normative reference: listed in CLSI standards for sensitivity testing, including media validation (Mueller-Hinton) and diffusion testing

7.9.6. Interpretation of Results

Analysis of Table 9 - Inhibition Diameters (mm)

The diameter of the inhibition zone is an indicator of antibacterial activity

- Large diameter → high activity (sensitive bacteria)
- Small diameter or absence of zone → low or no activity (resistant bacteria)

a) Staphylococcus aureus (ATCC 38213, G+)

- H_2L good activity (10 mm)
- $\{Fe(HL)(ClO_4)_2\}$: most marked activity (15 mm)

Conclusion: H_2L derivatives, especially $\{Fe(HL)(ClO_4)_2\}$, are the most active against S. aureus.

b) Escherichia coli (NCTC 25923, G–)

- $\{Fe(HL)(ClO_4)_2\}$: good activity (10 mm, identical but more regular)

Conclusion: *E. coli* is less sensitive overall, but H_2L and $\{Fe(HL)(ClO_4)_2\}$ maintain correct effectiveness.

c) Enterococcus faecalis (ATCC 29212, G+)

- Only $\{Fe(HL)(ClO_4)_2\}$shows activity (16 mm)

Conclusion: $\{Fe(HL)(ClO_4)_2\}$ is the only active molecule against E. faecalis.

d) Pseudomonas aeruginosa (ATCC 27853, G–)

- No compound shows activity.

Conclusion: P. aeruginosa remains fully resistant, which is expected because this bacteria is naturally multi-resistant.

e) Comparison with controls (Doripenem & Ceftriaxone)

- Doripenem: wide zones (23-32 mm) → very high activity
- Ceftriaxone: low activity on E. coli and E. faecalis (7-14 mm), no activity on S. aureus and P. aeruginosa.

Conclusion: the new molecules tested present modest to moderate activity, much lower than Doripenem but sometimes higher than Ceftriaxone in certain cases (notably E. faecalis with $\{Fe(HL)(ClO_4)_2\}$).

Analysis of Table 10 - Minimum Inhibitory Concentrations (MIC, mg/mL)

The MIC is the lowest concentration preventing bacterial growth.

- Low MIC → powerful molecule
- High MIC or ND → ineffective molecule

a) Staphylococcus aureus

$\{Fe(HL)(ClO_4)_2\}$: ND → not tested or not active

- Escherichia coli

H_2L: MIC = 10 mg/mL (low activity)

Conclusion: limited effectiveness against *E. coli*, requiring higher doses.

b) Enterococcus faecalis

- All ND except control → no inhibition detected.

Conclusion: despite the activity observed with $\{Fe(HL)(ClO_4)_2\}$, the MIC was not determined (perhaps linked to an experimental limit).

c) Pseudomonas aeruginosa

- All ND → confirmation of the absence of activity.

Overall Interpretation

- Best candidates

- {Fe(HL)$(ClO_4)_2$} is active on *S. aureus* and especially *E. faecalis* (zone 16 mm).
- H_2L: active on *S. aureus* and *E. coli* (MIC 5-10 mg/mL).
- Limited activity

Conclusion: The {Fe(HL)$(ClO_4)_2$} derivative appears to be the most promising, particularly against *Enterococcus faecalis*, which is often difficult to treat.

7.9.7. Comparative Antibacterial Discussion

The antibacterial performance of the pyridine-hydrazone ligand HL and its lanthanide(III) complexes can be usefully contrasted with that of the Schiff base ligand H_2L and its iron(III) complex, {Fe(HL)$(ClO_4)_2$}, tested in the present work. Although the two series were evaluated under partly different experimental protocols (agar well diffusion with MIC determination for the HL/Ln(III) series versus disc diffusion combined with a separate MIC assay for the H_2L/Fe(III) system), a qualitative and quantitative comparison-including conversion of MIC values to molar concentrations-highlights several informative trends regarding the influence of the metal center and the coordination environment on antibacterial potency.

Activity against Escherichia Coli

The HL/lanthanide series displayed markedly superior activity against *E. coli* compared with the H_2L/Fe(III) system. On a mass basis, the La(III) and Pr(III) complexes achieved the lowest MIC values recorded in this study (0.047 mg mL^{-1}), roughly 200-fold lower than the MIC obtained for H_2L (10 mg mL^{-1}). Converting to molar concentrations confirms that this advantage is not a molecular-weight artefact: La and Pr remain tied as the most potent complexes on a molar basis (0.139 mM each), some 200-fold below the molar MIC of H_2L (29.8 mM). Even the least active lanthanide complexes (Tb, Nd; MIC ≈ 0.52-0.55 mM) remained substantially more potent than the H_2L/Fe(III) system against this Gram-negative strain.

Activity against Pseudomonas Aeruginosa

The most striking contrast between the two series concerns *P. aeruginosa*, a Gram-negative organism noted for intrinsic multidrug resistance. All nine lanthanide complexes retained measurable activity (MIC range: 0.253-1.108 mM), whereas both H_2L and its iron(III) complex were completely inactive against this strain (NA). On a molar basis, Yb(III) emerges as the single most potent complex against this strain (0.253 mM), narrowly ahead of Eu(III) and Sm(III) (0.268-0.270 mM)-a distinction not evident from the mass-concentration data alone, where Eu, Yb, La, Pr and Sm appeared essentially equivalent. This divergence indicates that the lanthanide coordination sphere confers an ability to overcome the outer-membrane permeability barrier of *P. aeruginosa* that is not shared by the iron(III) complex.

Activity against Staphylococcus Aureus

Against this Gram-positive strain, the HL/lanthanide complexes again outperformed the H_2L system on a molar basis: Yb(III) was the most active (2.02 mM), closely followed by Eu(III) (2.14 mM) and Sm(III) (2.15 mM), all well below the molar MIC of H_2L (14.9 mM). Interestingly, when assessed by the disc diffusion method, {Fe(HL)$(ClO_4)_2$} produced the largest inhibition zone recorded across the entire H_2L series (15 mm), exceeding that of the free ligand (10 mm). This apparent discrepancy underscores an important methodological point: inhibition zone diameter and MIC report related but distinct aspects of antibacterial behaviour (diffusion efficiency through agar versus intrinsic growth-inhibitory concentration), and direct cross-comparison between compounds evaluated by different assays should be made with appropriate caution.

Activity Against Enterococcus Faecalis

This strain was assessed only within the H_2L series, where {Fe(HL)$(ClO_4)_2$} was the sole compound to show any inhibitory activity (16 mm inhibition zone), while free H_2L exhibited only weak activity (7 mm). Although the MIC for {Fe(HL)$(ClO_4)_2$} against *E. faecalis* could not be determined in the present assay, the disc diffusion result identifies this iron(III) complex as a promising candidate against a Gram-positive species frequently associated with resistant nosocomial infections.

Effect of Metal Coordination

Considered together, the two datasets support the general principle, consistent with Tweedy's chelation theory, that coordination to a metal centre can enhance the antibacterial activity of a hydrazone-type ligand relative to the free +ligand, as observed for La(III)/Pr(III) against *E. coli* and for {Fe(HL)$(ClO_4)_2$} against *S. aureus* and *E. faecalis*. However, this enhancement is not universal: several lanthanide complexes (Ce, Nd, Tb) showed reduced activity relative to free HL against *P. aeruginosa*, indicating that the effect of chelation is strongly dependent on both the identity of the metal ion and the bacterial strain under investigation, rather than reflecting a uniform mechanism of enhanced membrane penetration or bioavailability upon complexation.

Table 12. MIC values of HL, its lanthanide(III) complexes and H_2L, expressed in mg mL^{-1} and mM.

Strain	Parameter	HL	La	Pr	Eu	Yb	Sm	Ce	Nd	Tb/Er*	H_2L
E. coli	MIC (mg/mL)	0.094	0.047	0.047	0.094	0.187	0.094	0.094	0.187	0.187/0.094	10
	MIC (mM)	0.474	0.139	0.139	0.268	0.504	0.270	0.278	0.546	0.524/0.257	29.8
P. aeruginosa	MIC (mg/mL)	0.094	0.094	0.094	0.094	0.094	0.094	0.375	0.375	0.375/0.187	ND
	MIC (mM)	0.474	0.279	0.277	0.268	0.253	0.270	1.108	1.095	1.050/0.512	ND

S. aureus	MIC (mg/mL)	0.75	0.75	0.75	0.75	0.75	0.75	>0.75	>0.75	>0.75/>0.75	5
	MIC (mM)	3.78	2.22	2.21	2.14	2.02	2.15	>2.22	>2.19	>2.10/>2.05	14.9

**Tb and Er values are given together (Tb/Er) as they were reported jointly in the source data. ND = not determined (molar mass of {Fe(HL)(ClO$_4$)$_2$} known, but MIC not determined for this complex). Shaded cells indicate the most potent value (lowest MIC) within each row for the lanthanide series.*

Table 13. Inhibition zone diameters (mm) for H_2L and {Fe(HL)(ClO$_4$)$_2$}, disc diffusion method.

Strains	H_2L inhibition zone (mm)	{Fe(HL)(ClO$_4$)$_2$} inhibition zone (mm)	Doripenem (mm)	Ceftriaxone (mm)
S. aureus ATCC 38213	10	15	28	NA
E. coli NCTC 25923	10	10	23	14
E. faecalis ATCC 29212	7	16	32	7
P. aeruginosa ATCC 27853	NA	NA	25	NA

NA = No Activity. Shaded cells indicate strains for which {Fe(HL)(ClO$_4$)$_2$} outperformed the free ligand H_2L.

8. Antioxidant Activity of the H_2L Ligand and Its Iron(III) Complex

The antioxidant activities of the ligand (E)-1-(pyridin-2-yl)-2-(pyridin-2-ylmethylene)hydrazone (HL) and its lanthanide complexes with Nd(III), Sm(III), Tb(III), Er(III), Ce(III), and Pr(III) were comprehensively investigated by M. Ndiaye-Gueye *and al.* [32]. using ascorbic acid as the reference antioxidant. The antioxidant capacity of the synthesized compounds was evaluated using the (DPPH•) radical scavenging assay, one of the most widely employed methods for assessing the free-radical scavenging ability of organic and inorganic compounds [38,39]. The assay is based on the reduction of the stable purple-colored DPPH• radical by an antioxidant capable of donating either a hydrogen atom or an electron, leading to the formation of the non-radical yellow-colored hydrazine (DPPH-H). Consequently, the decrease in absorbance at 517 nm is directly proportional to the radical-scavenging capacity of the tested compound. The antioxidant activity was expressed as the radical scavenging activity (RSA, %) according to the following equation [40]:

$$Scavenging\ activity\ (\%\ of\ control) = \frac{(control\ activity - sample\ activity)}{sample\ activity} \times 100$$

All measurements were performed in triplicate, and ascorbic acid was used as the positive control. Initially, the antioxidant activity of the free ligand HL was evaluated. Subsequently, considering the growing biomedical interest in lanthanide compounds, the corresponding Y(III), Gd(III), Er(III), Nd(III), Sm(III), Ce(III), and Pr(III) complexes were investigated to assess the influence of metal coordination on the antioxidant properties of the ligand.

The DPPH• solution exhibits a characteristic purple color with a maximum absorption at 517 nm. Upon reaction with an antioxidant, the DPPH• radical is converted into the reduced form (DPPH-H), resulting in a gradual decrease in absorbance. The reaction kinetics depend on the nature of the antioxidant employed [41]. The radical scavenging activities of all compounds were determined over a range of concentrations, and the corresponding dose–response curves were constructed by plotting the percentage inhibition against the sample concentration, using ascorbic acid as the reference standard. The IC_{50} values, defined as the concentration required to scavenge 50% of DPPH• radicals, were obtained graphically from the inhibition curves (Figures 3a-c). Ascorbic acid exhibited the strongest antioxidant activity, with an IC_{50} value of 0.980 ± 0.005 µM**.** The synthesized compounds also demonstrated significant DPPH radical scavenging activity, with IC_{50} values of 16.32 ± 0.03**,** 12.05 ± 0.04**,** 10.65 ± 0.02**,** 8.95 ± 0.01**,** 8.01 ± 0.01**,** and 3.72 ± 0.02**,** corresponding respectively to the free ligand HL and the Pr(III), Gd(III), Y(III), Er(III) and Ce(III) complexes. For all investigated compounds, the radical scavenging activity increased progressively with increasing concentration before reaching a plateau, as illustrated in Figures 3a and 3b. Among all synthesized complexes, the Ce(III) complex exhibited the lowest IC_{50} value, indicating the highest antioxidant activity. Although the antioxidant performance of the synthesized compounds remained lower than that of ascorbic acid, the coordination of HL with lanthanide(III) ions markedly enhanced its radical scavenging ability. The inhibitory effect increased rapidly within the concentration range of 0-50 µM**,** demonstrating a clear concentration-dependent antioxidant response. The enhancement observed after complexation may be explained by the electronic effect exerted by the coordinated lanthanide ion. Coordination through the azomethine nitrogen atom of the C=N–NH chromophoric group withdraws electron density from the ligand, thereby increasing the polarization of the N–H bond. This electronic redistribution facilitates hydrogen atom donation to the DPPH radical, resulting in improved radical scavenging efficiency [42]. Overall, all lanthanide complexes exhibited higher antioxidant activity than the free ligand, confirming the beneficial effect of metal coordination. Among the investigated compounds, the Ce(III) complex proved to be the most effective antioxidant. Furthermore, the results suggest a relationship between the antioxidant activity and the ionic radius of the lanthanide ions, with the antioxidant efficiency generally increasing as the ionic radius decreases across the lanthanide series.

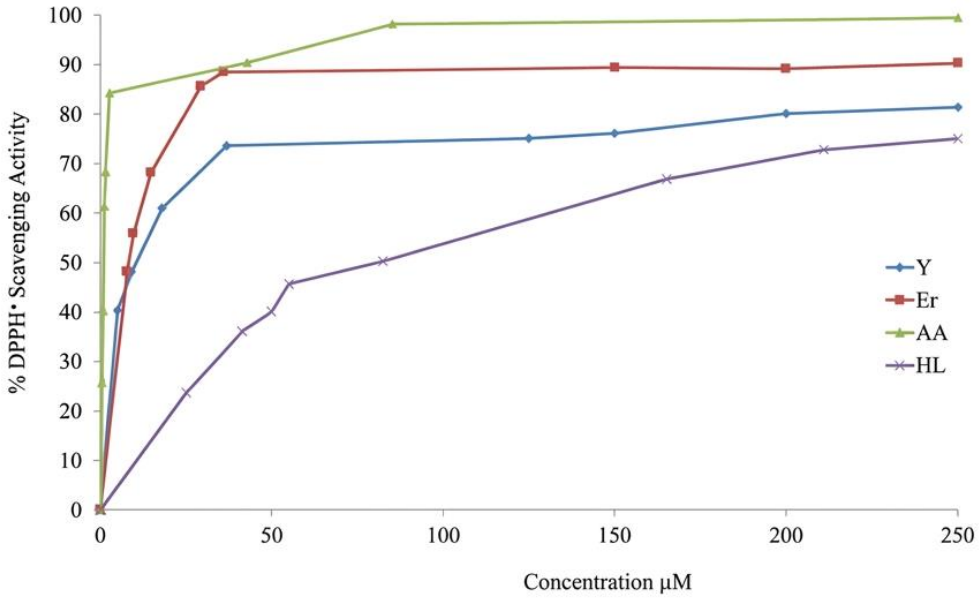

Fig. 3 (a) DPPH radical scavenging activity of (a) ascorbic acid (AA), HL, the Y(III) and Er(III) complexes

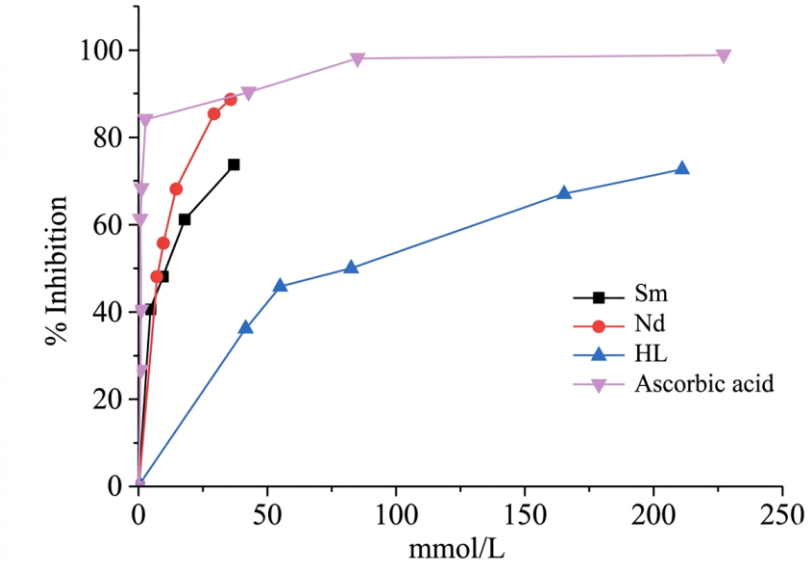

Fig. 3 (b) Ascorbic acid, HL, and the Nd(III) and Sm(III) complexes

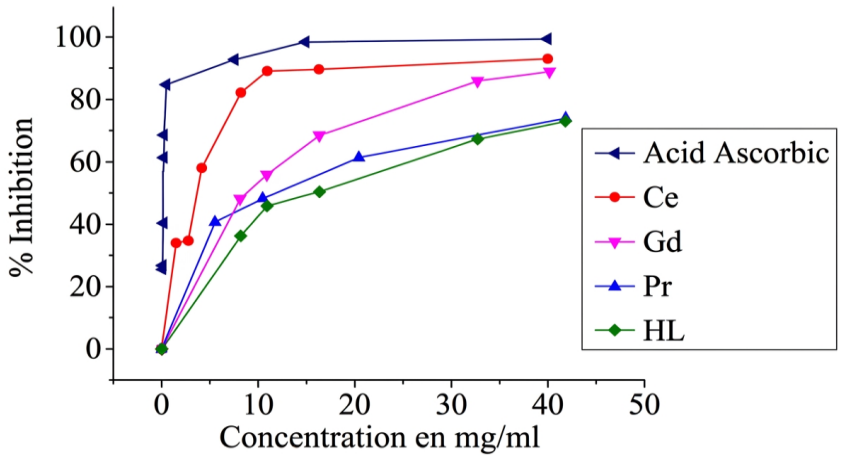

Fig. 3 (c) Ascorbic acid, HL, and the Ce(III), Gd(III), and Pr(III) complexes

In summary, the DPPH assay demonstrated that complexation of HL with lanthanide(III) ions significantly improves its antioxidant properties. The Ce(III) complex exhibited the highest radical scavenging capacity among the synthesized compounds, whereas the free ligand showed the lowest activity. These findings clearly indicate that lanthanide coordination enhances the electron- and hydrogen-donating ability of the hydrazone ligand, thereby increasing its antioxidant potential.

Following the structural, spectroscopic, and physicochemical characterization of the H_2L ligand and its iron(III) complex, it is important to evaluate the effect of metal coordination on its biological properties. Schiff base coordination compounds are well known for exhibiting a wide range of biological activities, which are often significantly influenced by both the nature of the metal ion and the coordination mode of the ligand.

In this context, the antioxidant activities of the free ligand and its metal complex were investigated to assess their radical-scavenging abilities. This study aims to establish a relationship between the structural features of the synthesized compounds and their potential antioxidant properties, thereby providing further insight into the influence of metal complexation on their biological performance.

The antioxidant activities of N'-[(1E)-1-(5-bromo-2-hydroxyphenyl)ethylidene]pyridine-3-carbohydrazide (H_2L) and its iron(III) complex were evaluated using the 2,2-diphenyl-1-picrylhydrazyl (DPPH•) radical-scavenging assay, with ascorbic acid serving as the reference antioxidant. The figure 4 illustrates the percentage of DPPH inhibition as a function of concentration for the free ligand and its iron(III) complex.

We first investigated the antioxidant activity of the ligand; then, to determine the influence of the metal center on its antioxidant capacity, we evaluated the antioxidant activity of the complex (table 14). Curves representing the percentage of inhibition versus sample concentration were plotted, and IC_{50} values were determined graphically (figure 4).

Table 14. Percentage of inhibition versus sample concentration.

	Concentration (mg/mL)	PI (%) H_2L	{Fe(HL)$(ClO_4)_2$}	PI (%) standard
	1	55.07	58.66	
	0.5	51.75	57.71	90.865
	0.25	45.48	55.07	88.011
	0.125	40.25	48.61	51.85
	0.0625	35.27	45.32	26.26
IC_{50}		0.577710265	0.222024185	0.1

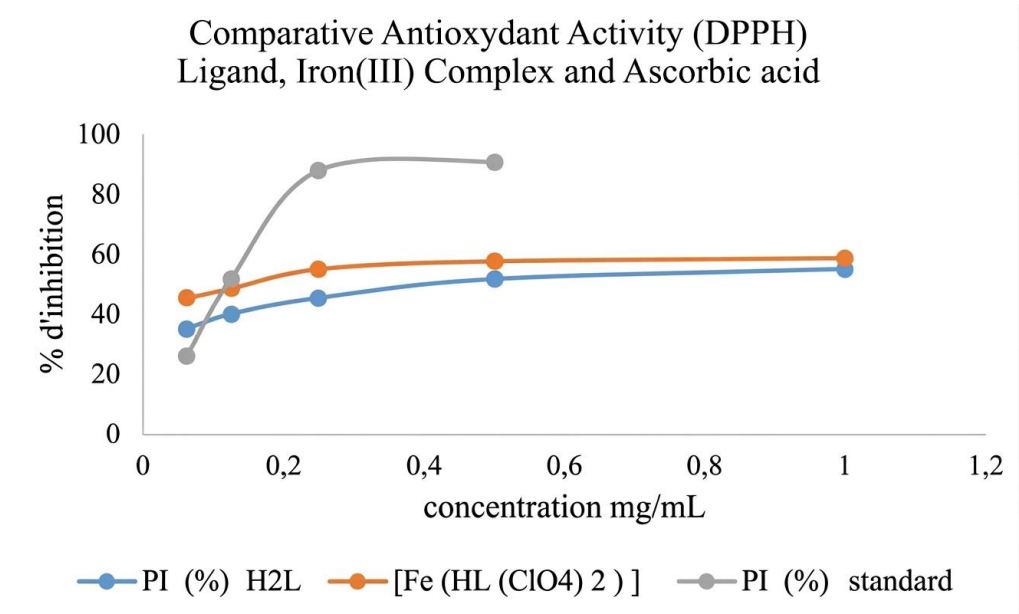

Fig. 4 DPPH radical-scavenging activities of H_2L and its iron(III) complex

Table 15. IC_{50} values and relative antioxidant activities of H_2L, its iron(III) complex, and ascorbic acid

Compounds	IC_{50} (mg/mL)	Relative antioxidant activity
Ascorbic acid	0.1	Very high
{Fe(HL)$(ClO_4)_2$}	2.6	Moderate to high
H_2L	4.8	Low

The inhibition curves clearly demonstrate the superior antioxidant activity of the reference compound while highlighting the beneficial effect of metal coordination on the radical-scavenging ability of the ligand [43]. Ascorbic acid reached 50% inhibition **(**IC_{50}**)** at a concentration of only 0.1 mg mL^{-1} and produced almost complete scavenging (approximately 95%) at 1 mg mL^{-1}. In comparison, the iron(III) complex exhibited an IC_{50} value of 2.6 mg mL^{-1}, whereas the free ligand showed a lower activity with an IC_{50} of 4.8 mg mL^{-1}. To further assess their antioxidant potential, the radical-scavenging activities of the free ligand and its iron(III) complex were compared with that of the commercial antioxidant ascorbic acid. The corresponding IC_{50} values are summarized in table 15**.**

The antioxidant activities decrease in the following order:

$$\text{Ascorbic acid} >> \{Fe(HL)(ClO_4)_2\} > H_2L.$$

Ascorbic acid exhibited the highest radical-scavenging activity owing to its well-established ability to donate hydrogen atoms and electrons readily, leading to the formation of the relatively stable dehydroascorbic acid and the efficient reduction of the DPPH• radical. Although the iron(III) complex remained less active than the reference antioxidant, its antioxidant capacity was markedly enhanced compared with that of the free ligand. The IC_{50} value decreased from 4.8 mg mL^{-1} for H_2L to 2.6 mg mL^{-1} after complexation, corresponding to an approximately 1.8-fold improvement in radical-scavenging efficiency.

The enhancement in antioxidant activity upon coordination can be attributed to the chelation effect, as described by Tweedy's chelation theory. Coordination of the ligand to the iron ion increases electron delocalization over the azomethine group and the conjugated aromatic system, which may facilitate electron or hydrogen atom transfer to the DPPH• radical. Furthermore, the presence of the Fe(III)/Fe(II) redox couple may contribute to the observed antioxidant activity through electron-transfer processes, although the relative contribution of this mechanism requires further investigation.

Overall, these results demonstrate that coordination of the Schiff base ligand with iron significantly enhances its antioxidant activity. While the iron(III) complex remains less active than ascorbic acid, metal complexation represents an effective strategy for improving the biological properties of Schiff base ligands and may contribute to the development of new bioactive coordination compounds.

8.1. Comparative Antioxidant Discussion

The antioxidant behavior of the pyridine-hydrazone ligand HL and its lanthanide(III) complexes can be compared with that of the Schiff base ligand H_2L and its iron(III) complex, $\{Fe(HL)(ClO_4)_2\}$, both evaluated by the DPPH• radical-scavenging assay using ascorbic acid as the reference standard. However, the IC_{50} value obtained for ascorbic acid differs by roughly two orders of magnitude between the two sub-studies (0.980 µM in the HL/lanthanide series versus ≈ 568 µM, i.e. 0.1 mg mL^{-1}, in the H_2L/Fe(III) series), indicating that the two assays were likely conducted under non-identical conditions (DPPH concentration, reaction time, or RSA calculation). Consequently, direct comparison of absolute IC_{50} values across the two series would be unreliable, and the discussion below instead relies on relative improvement factors-the fold-change in activity upon metal coordination, and the fold-difference relative to ascorbic acid within each series-which remain valid regardless of inter-assay protocol differences.

8.2. Improvement upon Metal Coordination

Within the HL/lanthanide series, coordination consistently enhanced radical-scavenging activity relative to the free ligand (IC_{50} = 16.32 µM), with improvement factors ranging from 1.35-fold for Pr(III) (IC_{50} = 12.05 µM) up to 4.39-fold for Ce(III) (IC_{50} = 3.72 µM), the most active complex identified in this study. Intermediate improvements were observed for Gd(III) (1.53-fold), Y(III) (1.82-fold), and Er(III) (2.04-fold). In the H_2L/Fe(III) system, coordination likewise improved activity, with the iron(III) complex (IC_{50} = 2.6 mg mL^{-1}) showing a 1.85-fold enhancement over free H_2L (IC_{50} = 4.8 mg mL^{-1}). This places the magnitude of improvement for $\{Fe(HL)(ClO_4)_2\}$ within the same general range as the more modestly enhanced lanthanide complexes (Pr, Gd, Y), though below that achieved by Ce(III).

8.3. Activity Relative to Ascorbic Acid

Within each series considered independently, all tested compounds remained less active than the reference antioxidant, consistent with the general expectation that ascorbic acid's enediol structure allows near-instantaneous sequential hydrogen donation. In the HL/lanthanide series, the free ligand was approximately 17-fold less active than ascorbic acid, a gap that narrowed to approximately 4-fold for the Ce(III) complex, the smallest gap to the reference standard among all compounds discussed here. In the H_2L/Fe(III) series, free H_2L was approximately 48-fold less active than ascorbic acid, narrowing to approximately 26-fold for $\{Fe(HL)(ClO_4)_2\}$ upon complexation.

8.4. Proposed Mechanism

Both series attribute the enhancement in radical-scavenging capacity upon coordination to a chelation-driven electronic effect consistent with Tweedy's theory. For the HL/lanthanide complexes, coordination through the azomethine nitrogen of the C=N–NH chromophore withdraws electron density from the ligand, increasing N–H bond polarization and facilitating hydrogen-atom donation to the DPPH• radical. For $\{Fe(HL)(ClO_4)_2\}$, a comparable mechanism is proposed, involving increased electron delocalization over the azomethine group and the conjugated aromatic system, with the additional possibility of a Fe(III)/Fe(II) redox contribution to radical scavenging-a pathway with no lanthanide counterpart, since the Ln(III) oxidation state investigated here is redox-stable under these conditions. This redox-active contribution, if confirmed, would represent a mechanistically distinct route to

antioxidant activity in the iron system relative to the purely ligand-centered hydrogen-donation mechanism proposed for the lanthanide series.

8.5. Trend Across the Lanthanide Series

Among the HL/lanthanide complexes, antioxidant efficiency was reported to increase broadly with decreasing ionic radius across the series, with Ce(III)-despite being one of the larger lanthanide ions among those tested-showing unexpectedly the strongest activity, suggesting that factors beyond ionic radius alone (such as the accessibility of the Ce(IV)/Ce(III) redox couple) may also contribute to its superior radical-scavenging performance.

Table 16. Relative antioxidant performance of HL, its lanthanide(III) complexes, and H_2L/{$Fe(HL)(ClO_4)_2$}, expressed as fold-change relative to the free ligand and to ascorbic acid within each series.

Series	Compound	IC_{50}	Fold-improvement vs. free ligand	Fold-less-active than ascorbic acid
HL/Ln	Ascorbic acid	0.980 µM	-	1 (reference)
HL/Ln	HL (free)	16.32 µM	1 (reference)	16.7×
HL/Ln	Pr(III)	12.05 µM	1.35×	12.3×
HL/Ln	Gd(III)	10.65 µM	1.53×	10.9×
HL/Ln	Y(III)	8.95 µM	1.82×	9.1×
HL/Ln	Er(III)	8.01 µM	2.04×	8.2×
HL/Ln	Ce(III)	3.72 µM	4.39×	3.8×
HL/Ln	Nd(III)	ND	ND	ND
HL/Ln	Sm(III)	ND	ND	ND
HL/Ln	Tb(III)	ND - inclusion unconfirmed	-	-
H_2L/Fe	Ascorbic acid	0.1 mg mL^{-1}	-	1 (reference)
H_2L/Fe	H_2L (free)	4.8 mg mL^{-1}	1 (reference)	48×
H_2L/Fe	{$Fe(HL)(ClO_4)_2$}	2.6 mg mL^{-1}	1.85×	26×

ND = not determined / not reported in the source text. The shaded row indicates the most active lanthanide complex (Ce(III)). Rows shaded in light grey correspond to compounds with unconfirmed or missing data.

9. Conclusion

The hydrazone Schiff base H_2L and its iron(III) complex were successfully synthesized and characterized by single-crystal X-ray diffraction of the ligand, IR, UV-Vis, and NMR spectroscopy, along with molar conductivity measurements. IR data confirmed that coordination proceeds via amide-iminol tautomerization and deprotonation, with the ligand binding through the iminol oxygen, azomethine nitrogen, and pyridine nitrogen atoms to form a stable, octahedral, non-electrolytic iron(III) complex. DPPH assays showed that metal coordination markedly enhanced antioxidant activity, with the complex (IC_{50} = 2.6 mg mL^{-1}) nearly twice as effective as the free ligand (4.8 mg mL^{-1}), though still less active than ascorbic acid. These results underscore the value of hydrazone Schiff bases as versatile ligands for bioactive iron(III) complexes and offer insight into the structure-coordination-activity relationship, supporting the rational design of new coordination compounds with improved biological properties.

References

[1] Yi Zhang et al., "Dual-Functions of the Carbon-Confined Oxygen on the Capacitance and Cycle Stability Enhancements of Zn-Ion Capacitors," *Journal of Materials Science and Technology*, vol. 221, pp. 278-288, 2025. [CrossRef] [Google Scholar] [Publisher Link]

[2] W. Chen et al., "Ultrahigh-Strength Cu-10Fe-0.2Mg in Situ Composites Via Ultra-Nano Precipitation within Nanolamellar Architectures," *Vacuum*, vol. 240, 2025. [CrossRef] [Google Scholar] [Publisher Link]

[3] Mustafa Bingöl, and Nevin Turan, "Schiff base and Metal(II) Complexes Containing Thiophene-3-Carboxylate: Synthesis, Characterization and Antioxidant Activities," *Journal of Molecular Structure*, vol. 1205, 2020. [CrossRef] [Google Scholar] [Publisher Link]

[4] Anu Kajal et al., "Therapeutic Potential of Hydrazones as Anti-Inflammatory Agents," *International Journal of Medicinal Chemistry*, vol. 2014, no. 1, pp. 1-11, 2014. [CrossRef] [Google Scholar] [Publisher Link]

[5] K. Siddappa, Sunilkumar B. Mane, and Deene Manikprabhu, "La(III) Complex Involving the O,N-Donor Environment of Quinazoline-4(3H)-One Schiff's base and Their Antimicrobial Attributes Against Methicillin-Resistant *Staphylococcus Aureus* (MRSA)," *Spectrochimica Acta Part A : Molecular and Biomolecular Spectroscopy*, vol. 130, pp. 634-638, 2014. [CrossRef] [Google Scholar] [Publisher Link]

[6] K.R. Joshi, A.J. Rojivadiya, and J.H. Pandya, "Synthesis and Spectroscopic and Antimicrobial Studies of Schiff base Metal Complexes Derived from 2-Hydroxy-3-Methoxy-5-Nitrobenzaldehyde," *International Journal of Inorganic Chemistry*, vol. 2014, no. 1, pp. 1-8, 2014. [CrossRef] [Google Scholar] [Publisher Link]

[7] Farba Bouyagui Tamboura et al., "Structural Studies of bis-(2,6-Diacetylpyridine-bis-(Phenylhydrazone)) and X-ray Structure of its Y(III), Pr(III), Sm(III) and Er(III) Complex," *Polyhedron*, vol. 23, no. 7, pp. 1191-1197, 2004. [CrossRef] [Google Scholar] [Publisher Link]

[8] Tudor Rosu et al., "Some New Cu(II) Complexes Containing an ON Donor Schiff base: Synthesis, Characterization and Antibacterial Activity," *Polyhedron*, vol. 30, no. 1, pp. 154-162, 2011. [CrossRef] [Google Scholar] [Publisher Link]

[9] Mbosse Ndiaye-Gueye et al., "Syntheses, Characterization, and X-ray Crystal Structure of Binuclear Lanthanide Complexes Assembled with Schiff base and Acetate," *Earthline Journal of Chemical Sciences*, vol. 7, no. 1, pp. 81-95, 2021. [CrossRef] [Google Scholar] [Publisher Link]

[10] Songul Duman, İrfan Kizilcikli, and Bahri Ülküseven, "Dioxomolybdenum(VI) Complexes of 5-Bromo/3,5-Dibromo-Salicylaldehyde 4-(H/C_6 H_5)- *S* -Propyl-Thiosemicarbazones," *Phosphorus, Sulfur, and Silicon and the Related Elements*, vol. 190, no. 3, pp. 342-351, 2015. [CrossRef] [Google Scholar] [Publisher Link]

[11] Marina Cindrić et al., "Synthesis and Characterization of Some Mono- and Dinuclear Molybdenum(VI) Thiosemicarbazonato Complexes," *Polyhedron*, vol. 24, no. 2, pp. 369-376, 2005. [CrossRef] [Google Scholar] [Publisher Link]

[12] Kamran T. Mahmudov et al., "New Copper(II) Dimer with 3-(2-Hydroxy-4-Nitrophenylhydrazo) Pentane-2, 4-Dione and its Catalytic Activity in Cyclohexane and Benzyl Alcohol Oxidations," *Journal of Molecular Catalysis A: Chemical*, vol. 318, no. 1-2, pp. 44-50, 2010. [CrossRef] [Google Scholar] [Publisher Link]

[13] Carlos J. Carrasco et al., "Recent Developments in Amino Acid-derived Imidazole-, Imidazolium- and N-Heterocyclic Carbene-carboxylate Complexes," *Inorganica Chimica Acta*, vol. 557, pp. 1-11, 2023. [CrossRef] [Google Scholar] [Publisher Link]

[14] Ting Zhang et al., "Bridging Biodegradable Metals and Biodegradable Polymers: A Comprehensive Review of Biodegradable Metal–organic Frameworks for Biomedical Application," *Progress in Materials Science*, vol. 155, 2026. [CrossRef] [Google Scholar] [Publisher Link]

[15] Silvia H. Cardoso et al., "Synthesis and Antitubercular Activity of Isoniazid Condensed with Carbohydrate Derivatives," *Química Nova*, vol. 32, no. 6, pp. 1557-1560, 2009. [CrossRef] [Google Scholar] [Publisher Link]

[16] H. EL. Hamdani, and M. EL. Amane, "Preparation, Spectral, Antimicrobial Properties and Anticancer Molecular Docking Studies of New Metal Complexes [M(caffeine)$_4$] (PF_6)$_2$; M = Fe(II), Co(II), Mn(II), Cd(II), Zn(II), Cu(II), Ni(II)," *Journal of Molecular Structure*, vol. 1184, pp. 262-270, 2019. [CrossRef] [Google Scholar] [Publisher Link]

[17] Akiko Watanabe et al., "Multi-Path Magnetic Relaxation of Mono-Dysprosium(III) Single-Molecule Magnet with Extremely High Barrier," *Chemistry A European Journal*, vol. 17, no. 27, pp. 7428-7432, 2011. [CrossRef] [Google Scholar] [Publisher Link]

[18] M.F. Iskander, L. El Sayed, and M.A. Lasheen, "Coordination Compounds of Hydrazine Derivatives with Transition Metals. X. Cobalt(II) Aroylhydrazone Complexes," *Inorganica Chimica Acta*, vol. 16, pp. 147-157, 1976. [CrossRef] [Google Scholar] [Publisher Link]

[19] K. Suresh Babu et al., "Synthesis and In Vitro Study of Novel 7-*O*-acyl Derivatives of Oroxylin A as Antibacterial Agents," *Bioorganic and Medicinal Chemistry Letters*, vol. 15, no. 17, pp. 3953-3956, 2005. [CrossRef] [Google Scholar] [Publisher Link]

[20] C.N.R. Rao, Chemical Applications of Infrared Spectroscopy, Academic Press, 1963. [Online]. Available : https://openlibrary.org/works/OL18451753W/Chemical_applications_of_infrared_spectroscopy

[21] Kozo Nagano, Tsune Kinoshita, and Zenzo Tamura, "Metal Complexes of Isonicotinoylhydrazine and Related Compounds. III. Consecutive Formation Constants for Various Metal Ions by the pH Titration Method," *Chemical and Pharmaceutical Bulletin*, vol. 11, no. 8, pp. 999-1013, 1963. [CrossRef] [Google Scholar] [Publisher Link]

[22] Soma Sen et al., "Synthesis, Crystal Structures and Magnetic Studies of Dicyanamide Bridged Two New 1D Copper(II) Complexes," *Inorganica Chimica Acta*, vol. 360, no. 15, pp. 4085-4092, 2007. [CrossRef] [Google Scholar] [Publisher Link]

[23] Anayive Pérez-Rebolledo et al., "Metal Complexes of 2-Benzoylpyridine Semicarbazone: Spectral, Electrochemical and Structural Studies," *Journal of Molecular Structure: Theochem*, vol. 794, no. 1-3, pp. 18-23, 2006. [CrossRef] [Google Scholar] [Publisher Link]

[24] Shaik Mustafa et al., "Synthesis, Characterization, and Biological Activities of Pendant Arm-Pyridyltetrazole Copper(II) Complexes: DNA Binding/Cleavage Activity and Cytotoxic Studies," *Chemistry and Biodiversity*, vol. 12, no. 10, pp. 1516-1534, 2015. [CrossRef] [Google Scholar] [Publisher Link]

[25] C.H. Kane et al., "Synthesis and Characterization of Novel M(II) (M = Mn(II), Ni(II), Cu(II) or Zn(II)) Complexes with Tridentate N2,O-donor Ligand (E)-2-amino-N'-[1-(pyridin-2-yl)- Ethylidene]Benzohydrazide," *Bulletin of the Chemical Society of Ethiopia*, vol. 30, no. 1, pp. 101-110, 2016. [CrossRef] [Google Scholar] [Publisher Link]

[26] Farba B. Tamboura et al., "X-ray Structure and Spectroscopic Properties of Some Lanthanides(III) Complexes Derived from 2,6-Diacetylpyridine-bis(Benzoylhydrazone)," *Inorganic Chemistry Communications*, vol. 6, no. 8, pp. 1004-1010, 2003. [CrossRef] [Google Scholar] [Publisher Link]

[27] W.J. Geary, "The use of Conductivity Measurements in Organic Solvents for the Characterisation of Coordination Compounds," *Coordination Chemistry Reviews*, vol. 7, no. 1, pp. 81-122, 1971. [CrossRef] [Google Scholar] [Publisher Link]

[28] Ibrahima Diouf et al., "Antisickling Properties of Hydro-Alcoholic Extract of Ficus Abutilifolia Leaves," *Journal of African Association of Physicological Siences*, vol. 12, no. 2, pp. 31-37, 2024. [CrossRef] [Google Scholar] [Publisher Link]

[29] H. Zhou et al., "Synthesis, Crystal Structure, Electrochemical, EPR and Magnetic Properties of Dinuclear Complexes with an Okawa-style Unsymmetrical Diphenolato Schiff base Macrocyclic Ligand," *Polyhedron*, vol. 26, no. 13, pp. 3233-3241, 2007. [CrossRef] [Google Scholar] [Publisher Link]

[30] Samir Alghool, M. Sh. Zoromba, and Hanan F. Abd El-Halim, "Lanthanide Amino Acid Schiff base Complexes: Synthesis, Spectroscopic Characterization, Physical Properties and *in Vitro* Antimicrobial Studies," *Journal of Rare Earths*, vol. 31, no. 7, pp. 715-721, 2013. [CrossRef] [Google Scholar] [Publisher Link]

[31] G.M. Sheldrick, *SHELXTL-97*, *Program for the Refinement of Crystal Structures*, University of Gottingen, Gottingen, Germany, 1997. [Google Scholar]

[32] Mbosse Ndiaye-Gueye et al., "Synthesis, Characterization and Antioxidant Activity of Lanthanide (III) Complexes with Tridentate Schiff base Ligand. X-ray Crystal structure of the Ce(III) Complex," *Romanian Journal of Chemistry, Romanian Academy*, vol. 62, no. 1, pp. 35-41, 2017. [Google Scholar]

[33] S. Treki Amina, R. Merghem, and L. Dehimat, "Phytochemical Study and Evaluation of the Antibacterial Activity of a Labiatae: Thymus Hirtus," *Science and Technology*, pp. 25-29, 2009. [Google Scholar] [Publisher Link]

[34] F. Bssaibis, N. Gmira, and M. Meziane, "Antibacterial Activity of Dittrichia Viscosa (L.) W. Greuter," *Journal of Industrial, Sanitary, and Environmental Microbiology*, vol. 3, pp. 44-55, 2009. [Google Scholar]

[35] Christian Duraffourd, L. D'hervicourt, J.C. Lapraz, "Clinical Phytotherapy Notebooks Volume 1: Laboratory Tests, Galenics," *Éléments Therapeutiques Synergiques*, 1983. [Google Scholar]

[36] A.G. Ponce et al., "Antimicrobial Activity of Essential Oils on the Native Microflora of Organic Swiss Chard," *LWT--Food Science and Technology*, vol. 36, no. 7, pp. 679-684, 2003. [CrossRef] [Google Scholar] [Publisher Link]

[37] AAT Bioquest, IC50 Calculator. [Online]. Available: https://www.aatbio.com/tools/ic50-calculator

[38] V. Yu Tyurin et al., "The Electrochemical Approach to Antioxidant Activity Assay of Metal Complexes with Dipicolylamine Ligand, Containing 2,6-Di-Tert-Butylphenol Groups, based on Electrochemical DPPH-Test," *Journal of Electroanalytical Chemistry*, vol. 756, pp. 212-221, 2015. [Google Scholar]

[39] Souvik Roy, "Synthesis, Characterisation and Antioxidant Activity of Luteolin–Vanadium (II) Complex," *Food Chemistry*, vol. 173, pp. 1172-1178, 2015. [Google Scholar]

[40] Jing Deng, Wangyuan Cheng, and Yand Guangzhong, "A Novel Antioxidant Activity Index (AAU) for Natural Products using the DPPH Assay," *Food Chemistry*, vol. 125, no. 4, pp. 1430-1435, 2011. [Google Scholar]

[41] N. Ito et al., "Studies on Antioxidants: Their Carcinogenic and Modifying Effects on Chemical Carcinogenesis," *Food and Chemical Toxicology*, vol. 24, no. 10-11, pp. 1071-1082, 1986. [Google Scholar]

[42] Weijun Chen et al., "Antioxidant Property of Quercetin–Cr(III) Complex: The Role of Cr(III) Ion," *Journal of Molecular Structure*, vol. 918, no. 1-3, pp. 194-197, 2009. [Google Scholar]

[43] Abdoul Sall et al., "Synthesis, Spectroscopic Characterization, Crystal Structure of the Ligand N'-[(E)-(4-Hydroxy-3-Methoxybenzylidene)] Pyridine-3-Carbohydrazide : Antibacterial and Antioxidant Activities of Ligand and its Zinc(II) Complex," *Chemical Science International Journal*, vol. 35, no. 4, pp. 212-226, 2026. [Google Scholar]